Ca^{2+} and calpain mediate capsaicin-induced ablation of axonal terminals expressing transient receptor potential vanilloid 1

Received for publication, January 30, 2017, and in revised form, March 28, 2017 Published, Papers in Press, March 30, 2017, DOI 10.1074/jbc.M117.778290

Sheng Wang[‡1], Sen Wang[‡1], Jamila Asgar[‡], John Joseph[‡], Jin Y. Ro[‡], Feng Wei[‡], James N. Campbell[§], and Man-Kyo Chung[‡2]

From the [‡]Department of Neural and Pain Sciences, School of Dentistry, Program in Neuroscience, Center to Advance Chronic Pain Research, University of Maryland, Baltimore, Maryland 21201 and [§]Centrexion, Baltimore, Maryland 21202

Edited by F. Anne Stephenson

Capsaicin is an ingredient in spicy peppers that produces burning pain by activating transient receptor potential vanilloid 1 (TRPV1), a Ca^{2+}-permeable ion channel in nociceptors. Capsaicin has also been used as an analgesic, and its topical administration is approved for the treatment of certain pain conditions. The mechanisms underlying capsaicin-induced analgesia likely involve reversible ablation of nociceptor terminals. However, the mechanisms underlying these effects are not well understood. To visualize TRPV1-lineage axons, a genetically engineered mouse model was used in which a fluorophore is expressed under the TRPV1 promoter. Using a combination of these TRPV1-lineage reporter mice and primary afferent cultures, we monitored capsaicin-induced effects on afferent terminals in real time. We found that Ca^{2+} influx through TRPV1 is necessary for capsaicin-induced ablation of nociceptive terminals. Although capsaicin-induced mitochondrial Ca^{2+} uptake was TRPV1-dependent, dissipation of the mitochondrial membrane potential, inhibition of the mitochondrial transition permeability pore, and scavengers of reactive oxygen species did not attenuate capsaicin-induced ablation. In contrast, MDL28170, an inhibitor of the Ca^{2+}-dependent protease calpain, diminished ablation. Furthermore, overexpression of calpastatin, an endogenous inhibitor of calpain, or knockdown of calpain 2 also decreased ablation. Quantitative assessment of TRPV1-lineage afferents in the epidermis of the hind paws of the reporter mice showed that EGTA and MDL28170 diminished capsaicin-induced ablation. Moreover, MDL28170 prevented capsaicin-induced thermal hypoalgesia. These results suggest that TRPV1/Ca^{2+}/calpain-dependent signaling plays a dominant role in capsaicin-induced ablation of nociceptive terminals and further our understanding of the molecular mechanisms underlying the effects of capsaicin on nociceptors.

This study was supported by National Institutes of Health Grant R01 DE023846 (to M. K. C.) and Maryland Industrial Partnership Grant 5403 (to M. K. C.). The authors declare that they have no conflicts of interest with the contents of this article. The content is solely the responsibility of the authors and does not necessarily represent the official views of the National Institutes of Health.

This article contains supplemental Fig. 1 and Movies 1 and 2.

[1] Both authors contributed equally to this work.

[2] To whom correspondence should be addressed: Dept. of Neural and Pain Sciences, School of Dentistry, University of Maryland, 650 W. Baltimore St., 8-South, Baltimore, MD 21201. Tel.: 410-706-4452; Fax: 410-706-0865; E-mail: mchung@umaryland.edu.

Capsaicin and related vanilloids account for the spiciness of chili peppers and are well known to be specific agonists of the transient receptor potential vanilloid 1 (TRPV1),[3] a Ca^{2+}-permeable ion channel enriched in nociceptors (1). Systemic or local administration of capsaicin or resiniferatoxin (RTX) has been suggested as a therapy to treat multiple pathological pain conditions (2, 3). Topical capsaicin treatment provides months of relief for post-herpetic neuralgia and HIV-associated neuropathy (4). Capsaicin injected directly into the area of Morton's neuroma has been found to provide pain relief (5). Thus, topical or targeted injection of capsaicin is a valuable approach for treating pathological pain conditions. Despite these clear benefits, the mechanisms of capsaicin-induced analgesia are still largely unclear (reviewed in Refs. 3, 6, 7).

Defunctionalization of nociceptors following the application of vanilloids is attributed to either functional suppression or structural ablation of nociceptors. Capsaicin inhibits voltage-dependent sodium currents, mechanosensitive currents, and action potential discharge in sensory neurons (8–10). These effects may lead to functional insensitivity of nociceptors and short-term analgesia following capsaicin application. It is uncertain, however, whether these effects mediate prolonged analgesia over a period of weeks to months. Alternatively, capsaicin-induced analgesia involves structural changes in TRPV1-expressing nociceptors. Although injection of a high dose of vanilloid irreversibly ablates somata in sensory ganglia, relatively low doses of vanilloids injected into peripheral tissues induce ablation of nociceptive terminals in rodents and humans (11–15). Ablation of nociceptor terminals achieved by localized peripheral application of vanilloids is limited to the injected region and does not result in degeneration of neurons in sensory ganglia (11, 13). Peripherally administered capsaicin-induced ablation is reversible; recovery of afferent terminals is observed within 2–3 months in rodents and humans (12–14, 16). Localized reversible ablation of nociceptive terminals by capsaicin without degeneration of soma within ganglia occurs

[3] The abbreviations used are: TRPV, transient receptor potential vanilloid; DRG, dorsal root ganglia; RTX, resiniferatoxin; MFC, microfluidic chamber(s); VDCC, voltage-dependent Ca^{2+} channel(s); ER, endoplasmic reticulum; mPTP, mitochondrial permeability transition pore(s); ROS, reactive oxygen species; FCCP, carbonyl cyanide *p*-trifluoromethoxyphenylhydrazone; Veh, vehicle; ANOVA, analysis of variance; Cap, capsaicin; MDL, MDL28170.

over a time course approximating that of therapeutic relief in patients (5, 7).

Reports of cultured neuronal or non-neuronal preparations have proposed contributory mechanisms to capsaicin-induced "cell death" (reviewed in Refs. 6, 7). Capsaicin-induced cell death by vanilloids *in vitro* requires Ca^{2+} influx (17) and involves activation of Ca^{2+}-dependent proteases (18) and dysfunction of mitochondria (19). These mechanisms may explain capsaicin-induced death of somata within ganglia following high-dose systemic injection or intraganglionic injection of vanilloids (11). It is unclear, however, whether ablation of "nociceptive terminals" following peripheral administration occurs through similar mechanisms. Although apoptosis of neurons and selective degeneration of axons share common mechanisms, distinct pathways mediate the two processes (20). Recently, capsaicin-induced axonal degeneration was shown to be associated with Ca^{2+}-dependent fission of axonal mitochondria (21), which suggests a common mitochondrion-dependent mechanism. In our view, however, the mechanisms underlying capsaicin-induced axonal ablation are distinct from and should be determined independent of capsaicin-induced neuronal death.

In this study, we determined the relative contribution of Ca^{2+}-dependent mechanisms underlying capsaicin-induced ablation of TRPV1-lineage axons *in vitro* by using genetic labeling of nociceptive neurons and multicompartmental cultures combined with real-time time-lapse imaging and *in vivo* by axonal labeling in hind paw skin. Our results indicate that TRPV1/Ca^{2+}- and calpain-dependent signaling plays dominant roles in capsaicin-induced ablation of TRPV1-lineage nociceptive axonal terminals *in vitro* and *in vivo*. These findings add to our understanding of the molecular mechanisms of capsaicin-induced analgesia and should inform efforts to improve the therapeutic use of capsaicin.

Results

Capsaicin ablates TRPV1-lineage afferent terminals in vitro

We have established a model to quantitatively assess ablation of TRPV1-lineage nerve terminals *in vitro*. We crossed two genetically engineered mouse lines (TRPV1^{Cre} and ROSA$^{mT/mG}$) to obtain TRPV1-GFP mice, which express GFP selectively in TRPV1-lineage neurons and tdTomato in all other cells. These mice permit the monitoring of changes in TRPV1-lineage afferent terminals in real time. Dissociated sensory neurons from DRG of TRPV1-GFP mice were plated into multicompartmental microfluidic chambers (MFC), permitting manipulation of axons independent of their somata (22). After approximately 2 weeks, when the axons extended across the compartment, we performed time-lapse imaging of GFP- and tdTomato-expressing axons before and after application of capsaicin to the axonal compartment (supplemental Movie 1 and supplemental Movie 2). Upon addition of capsaicin (100 μM) to the axonal compartment, GFP-positive axons began to display blebbing or beading (Fig. 1, *C* (*arrow*) and *D*), disruption of continuity, fragmentation (Fig. 1, *C* and *D*, *arrowheads*), and detachment of axonal debris, which are typical signs of axonal degeneration (23, 24). Changes occurred as early as 1 min after capsaicin application, and ~60% of GFP-positive fibers exhibited blebbing or disruption after 10 min. In contrast, tdTomato-positive axons showed no changes upon capsaicin application (Fig. 1, *E*–*G*). These results indicate that capsaicin selectively breaks down the structure of axons of TRPV1-lineage fibers but not other fibers. To quantify the effects of capsaicin on axonal ablation, the proportions of unaffected GFP-positive fibers were calculated as exemplified in supplemental Fig. 1. The survival proportions were plotted to reflect time-dependent changes (Fig. 1*H*).

Because capsaicin was applied directly to the axonal chamber, it is likely that capsaicin-induced ablation of axonal terminals was localized to the axons within the axonal chamber and not a secondary consequence of initial degeneration of somata. To confirm proper segregation between soma and axon chambers, we quantified changes in axonal terminals within the axonal chamber following the application of 100 μM capsaicin to the soma chamber (Fig. 1*H*). This treatment only modestly affected axons in axonal chambers, and 90% of GFP-positive terminals were not affected after 20 min following capsaicin application to the soma chamber, suggesting that leakage between the two chambers was minimal. We also tested the possibility that axonal terminal ablation by capsaicin induced "dying back" degeneration or transganglionic degeneration. In microfluidic chambers with double axonal chambers, application of capsaicin on one side induced ablation of axonal terminals on that side but not on the contralateral side within a 30-min period (Fig. 1, *I* and *J*). These results indicate that this system could be used for real-time monitoring of capsaicin-induced changes in TRPV1-lineage afferent terminals without affecting the soma. We used this model to investigate the mechanisms underlying capsaicin-induced ablation of afferent terminals.

The effects of capsaicin were concentration-dependent (Fig. 2, *A*–*C*); the half-maximal concentration of capsaicin was 427 nM (95% confidence interval, 207–882 nM; Fig. 2*C*). RTX, another TRPV1 agonist, also induced ablation over the course of 30 min (Fig. 2*B*). The half-maximal concentration of RTX was 11.5 nM (95% confidence interval, 6–22 nM; Fig. 2*C*). Neither capsaicin nor RTX ablated more than 80% of TRPV1-lineage fibers, which is consistent with the fact that not all adult TRPV1-lineage neurons express TRPV1 (25).

Capsaicin-induced ablation of TRPV1-lineage afferent terminals depends on Ca^{2+} influx through TRPV1

To determine the mechanisms of capsaicin-induced ablation, we examined the survival of TRPV1-lineage nerve fibers treated with 100 μM capsaicin under various conditions (Fig. 3). We chose this concentration because the approximate concentrations of capsaicin based on the injected doses in humans range from 300–650 μM (5, 14). In addition, we intended to produce a maximum and more consistent extent and rate of ablation by using a supramaximal concentration of capsaicin. Because we performed real-time fluorescence imaging, more rapid and dramatic changes were preferred to monitor the changes of afferent terminals without any potential changes from somata located in the opposite side of the chamber. Because capsaicin-induced cell death is dependent on Ca^{2+} (17, 18), we investigated the involvement of Ca^{2+} in capsaicin-in-

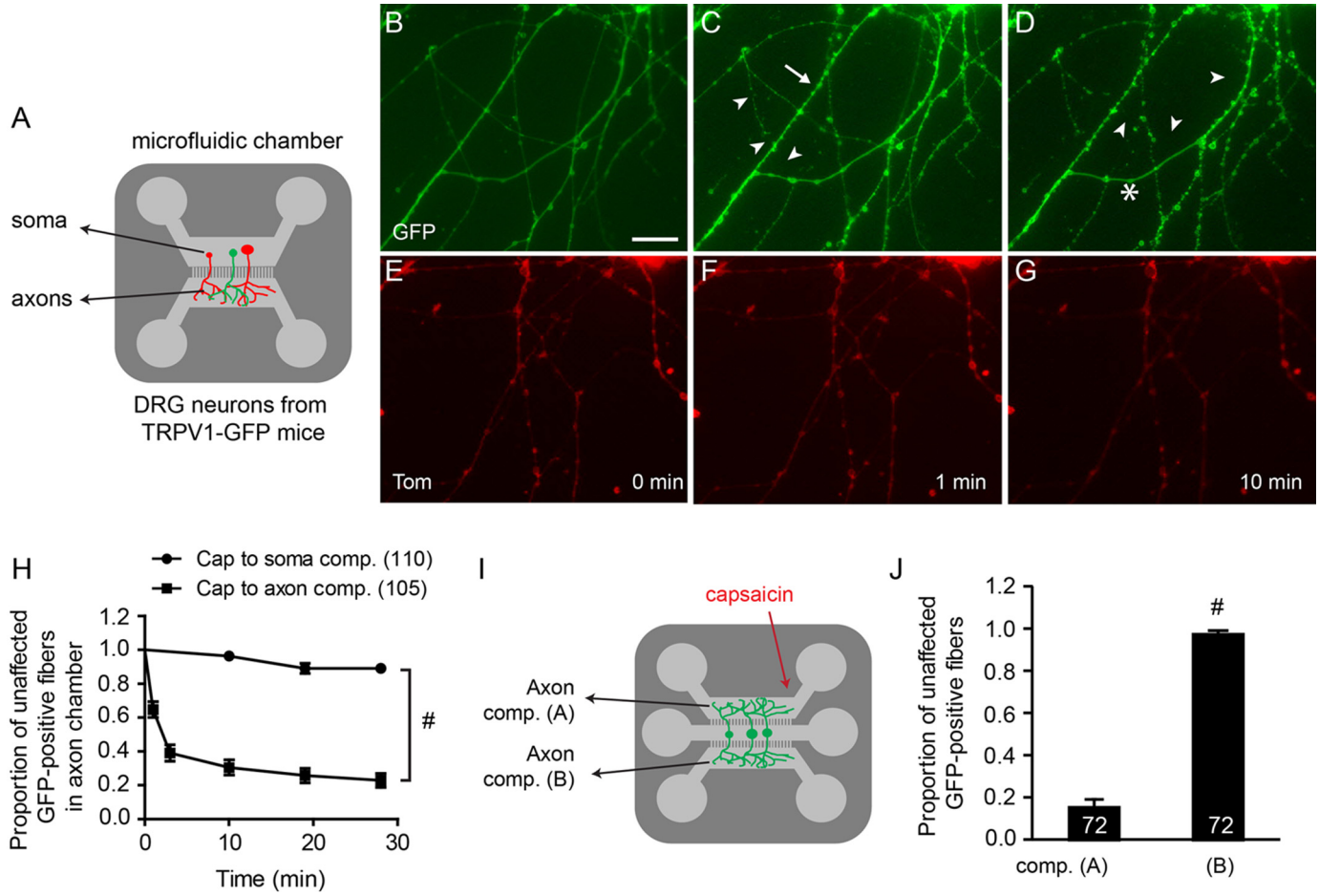

Figure 1. Capsaicin induces ablation of TRPV1-lineage axonal terminals. *A*, schematic of multicompartmental culture of DRG neurons in an MFC (Xona Microfluidics). Primary afferent neurons were dissociated from TRPV1-GFP reporter mice and plated in one side of the MFC. Axonal terminals cross the barrier and reach the compartment in the other side (axonal compartment). Capsaicin application was restricted to the axonal compartment, where time-lapse imaging was performed. *B*—*G*, representative time-lapse imaging of axonal terminals from MFC. Fluorescence signals from GFP (*B–D*) and tdTomato (*E–G*) were monitored before and after the axonal compartment was exposed to capsaicin (100 μM). *Scale bar* = 10 μm. *Arrowheads*, ablated fibers; *arrow*, beaded fibers; *asterisk*, fibers not affected. Movie files showing the entire field are available (supplemental Movies 1 and 2). *H*, proportion of unaffected fibers after application of 100 μM capsaicin to either somata (*circles*) or axonal compartments (*comp.*, *squares*). Survival proportion is plotted as mean ± S.E. *Numbers in parentheses* represent the numbers of individual GFP-expressing fibers examined in each group. Log-rank test; #, $p < 0.0001$. *I*, schematic of the multicompartmental culture of DRG neurons dissociated from TRPV1-GFP reporter mice in triple MFC. Time-lapse imaging was performed in axonal compartments A and B before and after application of 100 μM capsaicin. *J*, proportion of unaffected fibers 28 min after the application of 100 μM capsaicin to compartment A. Survival proportion is plotted as mean ± S.E. *Numbers within columns* represent the numbers of individual GFP-expressing fibers examined in each group. Log-rank test; #, $p < 0.0001$.

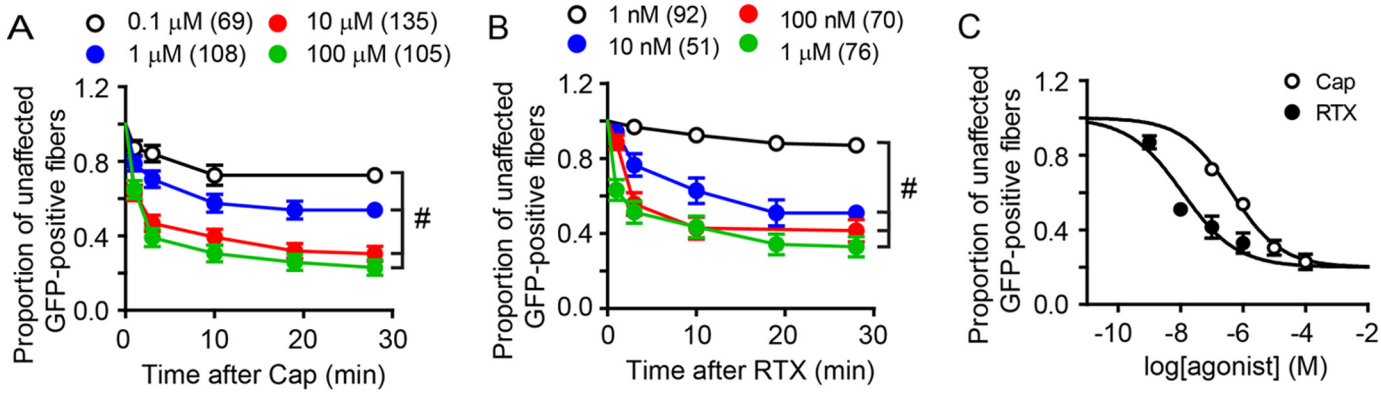

Figure 2. Capsaicin and RTX ablate TRPV1-lineage axonal terminals. *A* and *B*, proportion of unaffected fibers after application of four different concentrations of capsaicin (*A*) or resiniferatoxin (*B*). Survival proportion is plotted as mean ± S.E. *Numbers in parentheses* represent the numbers of individual GFP-expressing fibers examined in each group. Log-rank test; #, $p < 0.0001$. *C*, concentration dependence of ablation induced by capsaicin or RTX, evaluated 28 min following application. The curves are best fits using a sigmoidal equation. *Numbers in parentheses* represent the numbers of individual GFP-expressing fibers examined in each group. Cap: bottom = 0.2, top = 1, $\log(IC_{50}) = -6.37 \pm 0.10$, Hill slope = $-0.54 \pm 0.0.07$. RTX: bottom = 0.2, top = 1, $\text{Log}(IC_{50}) = -7.9 \pm 0.14$, Hill slope = -0.50 ± 0.08.

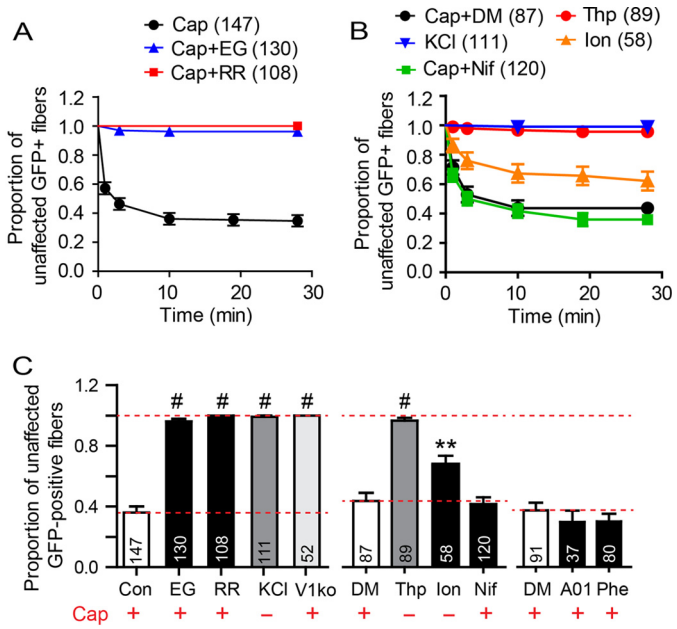

Figure 3. Capsaicin-induced ablation depends on Ca^{2+} influx through TRPV1. *A* and *B*, *in vitro* ablation assay in MFC was performed under the indicated conditions. *Cap*, 100 μM capsaicin; *EG*, 10 mM EGTA without addition of Ca^{2+}; *RR*, ruthenium red (a pore blocker of TRPV1), 10 μM; *KCl*, 50 mM KCl (substituted for 50 mM NaCl); *DM*, control with DMSO less than 0.1%; *Thp*, 2 μM thapsigargin (an inhibitor of ER Ca^{2+} ATPase); *Ion*, 5 μM ionomycin (a Ca^{2+} ionophore); *Nif*, 1 μM nifedipine (an L-type Ca^{2+} channel blocker). *Numbers in parentheses* represent the numbers of individual GFP-expressing fibers examined in each group. *C*, quantification and statistical analysis of the experiments in *A* and *B* and other conditions. Statistical comparison was performed throughout the entire 28-min time-course by log-rank test, but, for simplicity, only the survival fractions (mean ± S.E.) of unaffected GFP-positive fibers 10 min following treatment are shown. *Cap* +, application of 100 μM capsaicin; *Cap* −, no capsaicin application; *Con*, control without adding vehicle; *A01*, 10 μM T16Ainh-A01 (an inhibitor of ANO1, Ca^{2+}-activated Cl^- channel); *PH*, 100 μM 9-phenanthrol (an inhibitor of TRPM4, Ca^{2+}-activated cationic channel). All groups were tested using DRG neurons from TRPV1-lineage reporter mice except TRPV1 KO mice (*V1ko*). TRPV1 KO mice were tested following electroporation of cDNA encoding GFP into dissociated DRG neurons. Log-rank test; **, $p < 0.005$; #, $p < 0.0001$. *Numbers within columns* represent numbers of axons examined in each group.

duced ablation. Capsaicin-induced ablation in the MFC was almost completely prevented when external Ca^{2+} was removed by Ca^{2+} deprivation and addition of EGTA, a Ca^{2+} chelator (Fig. 3, *A* and *C*, *EG*), suggesting that Ca^{2+} influx upon TRPV1 activation was required for capsaicin-induced ablation. In addition to the chelation of extracellular Ca^{2+}, application of ruthenium red, an inhibitor of Ca^{2+} influx via the TRPV1 pore, tk;1 prevented ablation, suggesting the importance of TRPV1-mediated Ca^{2+} influx. Furthermore, capsaicin did not induce ablation in neurons from TRPV1 knock-out mice (V1ko), confirming TRPV1-dependent ablation. When ionomycin (Fig. 3, *Ion*), a Ca^{2+} ionophore, was applied without capsaicin, ablation of TRPV1-lineage afferent terminals occurred, which suggests that the intracellular Ca^{2+} increase is sufficient to initiate ablation. Following axotomy in *ex vivo* DRG explants, inhibition of L-type voltage-dependent Ca^{2+} channels (VDCC), but not N-type ones, attenuated axonal degeneration (26). However, blockade of L-type Ca^{2+} channels by nifedipine (Fig. 3, *Nif*) did not affect capsaicin-induced ablation in our model, which argues against a major role of VDCC in capsaicin-induced ablation. Consistently, ablation was not induced by the application of high-concentration KCl (Fig. 3, *KCl*), which increases intracellular Ca^{2+} levels by opening VDCC. Capsaicin induces Ca^{2+} release from the endoplasmic reticulum (ER) (27), and it is known that Ca^{2+} released from the ER contributes to Wallerian degeneration in the sciatic nerve (28). However, release of Ca^{2+} from the ER by application of thapsigargin (Fig. 3, *Thp*) did not induce ablation of TRPV1-lineage nerve terminals in the absence of capsaicin (Fig. 3). Ca^{2+} influx through TRPV1 is known to activate ANO1, a Ca^{2+}-activated Cl^- channel, which amplifies neuronal depolarization (29). It is also possible that TRPM4, a Ca^{2+}-activated cationic channel, is activated following Ca^{2+} influx and induces neuronal ablation (30). However, this does not appear to be the case, as neither T16Ainh-A01, an inhibitor of ANO1, nor 9-phenanthrol, an inhibitor of TRPM4, affected capsaicin-induced ablation. Overall, these results suggest that Ca^{2+} influx through TRPV1 provides necessary and sufficient Ca^{2+} for capsaicin-induced ablation and indicate that other sources of Ca^{2+}, such as Ca^{2+} influx through VDCC and Ca^{2+} release from the ER or other sources of neuronal excitation through Ca^{2+}-dependent Cl^- or cationic channels, are not dominant contributors.

Mitochondrial dysfunction is not a dominant contributor to capsaicin-induced ablation

Next we tested the contribution of mitochondrial dysfunction to capsaicin-induced ablation of nociceptive terminals. Ca^{2+} influx through TRPV1 following capsaicin application is sequestered in mitochondria in sensory neurons (31). It is well established that excessive Ca^{2+} loading into mitochondria can cause mitochondrial dysfunction, including opening of mitochondrial permeability transition pores (mPTP) or generation of reactive oxygen species (ROS) (32). These events are known to mediate the degeneration of sensory nerves following injury (33) and, hence, may be involved in capsaicin-induced ablation. Indeed, capsaicin-induced cell death of sensory neurons was attenuated by inhibition of mPTP by cyclosporin A (19). On the other hand, it was also suggested that capsaicin depolarizes mitochondrial membrane potential by direct action on mitochondria in sensory neurons (34), which potentially contributes to cytotoxicity. Furthermore, it was recently suggested that Ca^{2+}-dependent mitochondrial fission augments capsaicin-induced axonal degeneration (21). However, it is still unclear whether mitochondria play a dominant role in capsaicin-induced ablation of nociceptive afferent terminals and how mitochondria contribute to capsaicin-induced axonal ablation.

Initially, we investigated whether capsaicin induces mitochondrial Ca^{2+} changes in a TRPV1-dependent manner. We used Fura-2 and mito-LAR-GECO, a genetically encoded Ca^{2+} sensor specifically targeted into mitochondria, for simultaneous monitoring of Ca^{2+} changes in both the cytosol and mitochondria of DRG neuronal somata. We confirmed that capsaicin (10 and 100 μM) elevated cytosolic free Ca^{2+}, which was accompanied by a robust increase in mitochondrial Ca^{2+} in a subset of DRG neurons (Fig. 4, *A* and *C*). In contrast, in the subset of neurons showing no cytosolic Ca^{2+} increase upon capsaicin application, there was no significant change in mito-

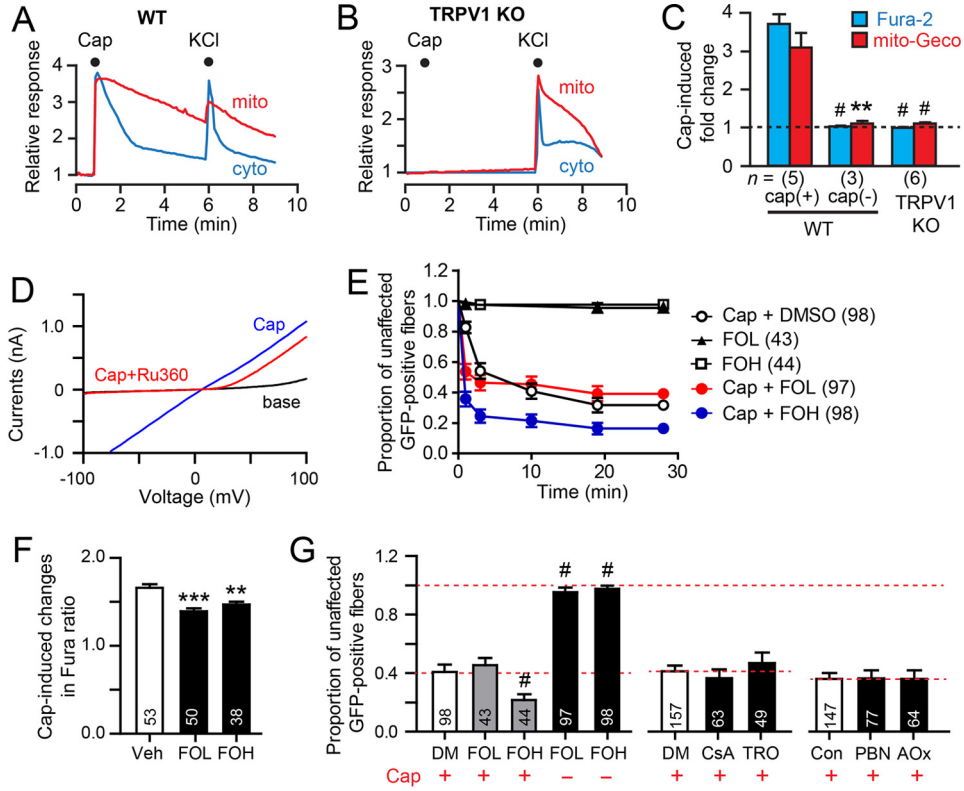

Figure 4. Depolarization of mitochondrial membrane potential, inhibition of mPTP, or ROS do not attenuate capsaicin-induced ablation of TRPV1-lineage nerve terminals. *A*—*C*, capsaicin induces Ca^{2+} loading into mitochondria in a TRPV1-dependent manner in somata of sensory neurons. Shown are representative relative traces of simultaneous recordings of cytosolic (*cyto*, *blue*) and mitochondrial (*mito*, *red*) Ca^{2+} levels in dissociated sensory neurons from WT (*A*) or TRPV1 KO mice (*B*). A genetically encoded Ca^{2+}-sensing protein targeted to mitochondria (LAR-GECO1.2) was electroporated into dissociated neurons. Ratiometric measurement of Fura-2/AM was performed in the same neurons to assess the cytosolic Ca^{2+} level. Cap (10 μM) followed by KCl (50 mM) was applied for 10 s at the indicated times. *C*, averaged Cap-induced changes normalized to the prestimulus baseline. *cap(+)*, WT neurons responding to capsaicin; *cap(−)*, WT neurons not responding to capsaicin. **, $p < 0.01$; #, $p < 0.001$ in Student's *t* test *versus* WT cap(+). *Numbers in parentheses* represent the numbers of neurons examined in each group. *D*, representative traces of whole-cell currents before (*black*) and after application of 1 μM capsaicin without (*blue*) or with (*red*) 10 μM Ru360 in HEK293 cells expressing TRPV1. *E*, *in vitro* ablation assay in MFC was performed under the indicated conditions. *Cap*, 100 μM capsaicin; *FOL*, 50 nM FCCP + 1 μM oligomycin; *FOH*, 0.5 μM FCCP + 1 μM oligomycin. *Numbers in parentheses* represent the numbers of individual GFP-expressing fibers examined in each group. *F*, changes in Fura ratio by 10 μM capsaicin following pretreatment of somata of dissociated DRG neurons under the indicated conditions. One-way ANOVA followed by Dunnett's post-hoc test; **, $p < 0.005$; ***, $p < 0.001$. *Numbers within columns* represent the numbers of neurons quantified in each group. *G*, quantification and statistical analysis of the experiments in *E* and other conditions. Statistical comparison was performed throughout the entire 28-min time course by log-rank test, but, for simplicity, only the survival fractions (mean ± S.E.) of unaffected GFP-positive fibers 10 min following treatment are shown. *Cap* +, application of 100 μM capsaicin; *Cap* −, no capsaicin application; *Con*, control without adding vehicle; *DM*, DMSO; *CsA*, 3 μM cyclosporin A (an inhibitor of mPTP); *TRO*, 10 μM TRO19622 (an inhibitor of mPTP); *PBN*, 2 mM phenyl a-*tert*-butyl nitrone (a ROS scavenger); *AOx*, antioxidant supplement (an anti-oxidant mixture with a proprietary composition). Log-rank test; #, $p < 0.0001$. *Numbers within columns* represent the numbers of GFP-expressing axons quantified in each group.

chondrial Ca^{2+} levels, suggesting that capsaicin-induced changes in mitochondrial Ca^{2+} are coupled with TRPV1 expression. Consistent with these results, DRG neurons derived from TRPV1 KO mice showed no changes in cytosolic or mitochondrial Ca^{2+} despite robust increases in both signals following KCl application (Fig. 4, *B* and *C*). These results suggest that capsaicin induces Ca^{2+} loading of mitochondria in a TRPV1-dependent manner and indicate that there are no changes in mitochondrial Ca^{2+} induced by capsaicin in the absence of functional TRPV1.

To test whether capsaicin-induced Ca^{2+} overloading of mitochondria mediates nerve terminal ablation, we sought to test the consequence of selective inhibition of Ca^{2+} uptake. However, a direct test was not possible because Ru360, the most widely used mitochondrial Ca^{2+} uptake inhibitor, directly inhibited TRPV1 (Fig. 4*D*). Capsaicin-evoked currents in HEK293 cells expressing TRPV1 were suppressed as much as 97.8% by 10 μM Ru360 at −60 mV ($n = 4$). Therefore, we indirectly examined the contribution of mitochondrial Ca^{2+} by pharmacologically depolarizing mitochondrial membrane potential. Carbonyl cyanide *p*-trifluoromethoxyphenylhydrazone (FCCP) eliminates mitochondrial membrane potential and induces release of Ca^{2+} from mitochondria to the cytosol, which is followed by prevention of mitochondrial Ca^{2+} uptake. FCCP attenuates glutamate-induced neuronal death in rat forebrain neurons (35), but it is not known whether FCCP diminishes axonal ablation. Because FCCP also depletes ATP synthesis, oligomycin (1 μM) was added in combination with FCCP (36). Although FCCP increases intracellular Ca^{2+} in sensory neurons robustly (data not shown) (37), 50 nM or 0.5 μM FCCP in combination with oligomycin by itself did not cause substantial ablation of nerve terminals (Fig. 4, *E* and *G*). When the axons were pretreated with FCCP/oligomycin, capsaicin-induced ablation was not attenuated. On the contrary, the rate of ablation was actually facilitated in both 50 nM and 0.5 μM concentrations, and the extent was more profound at 0.5 μM

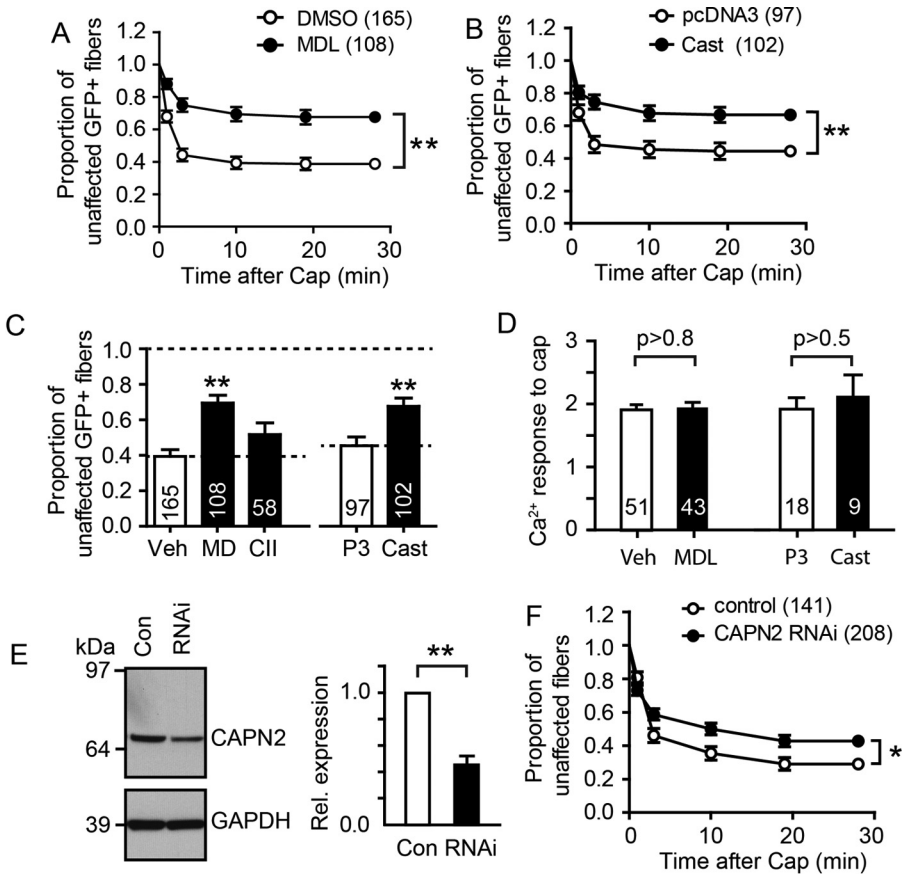

Figure 5. Inhibition of calpain attenuates capsaicin-induced ablation. *A* and *B*, time course of capsaicin-induced ablation of TRPV1-lineage nerve fibers in the presence of MDL or DMSO (*A*) or following transfection human calpastatin (*Cast*) or pcDNA3 (*P3*, *B*). Log-rank test; *, $p < 0.05$; **, $p < 0.005$. *Numbers in parentheses* represent the numbers of individual GFP-expressing fibers examined in each group. *C*, quantification of the *in vitro* ablation assay in MFC under the indicated conditions. Survival fraction (mean ± S.E.) of unaffected GFP-positive fibers 10 min following treatment with three calpain inhibitors are plotted. *Veh*, DMSO control; *CII*, 10 μM calpain inhibitor I; *MDL*, 10 μM MDL28170. Log-rank test; **, $p < 0.01$. *Numbers within columns* represent the numbers of axons quantified in each group. *D*, capsaicin-induced change of Fura ratio in somata of dissociated sensory neurons under the indicated conditions. *Numbers within columns* represent the numbers of neurons quantified in each group. *E*, *left panel*, representative Western blot of calpain 2 (*Capn2*) in dissociated DRG cultures following treatment with RNAi against calpain 2 or control (*Con*). *Right panel*, relative expression of calpain2 in the RNAi-treated group normalized to control. $n = 4$, $p < 0.05$, Student's *t* test. *F*, time course of capsaicin-induced ablation of TRPV1-lineage nerve fibers following treatment with RNAi against calpain 2. Log-rank test; *, $p < 0.05$. *Numbers in parentheses* represent the numbers of individual GFP-expressing fibers examined in each group.

concentration (Fig. 4, *E* and *G*). This facilitation was not due to enhanced activation of TRPV1 because pretreatment of dissociated sensory neurons with FCCP/oligomycin slightly attenuated the extent of intracellular Ca^{2+} increase within somata following capsaicin-induced activation of TRPV1 (Fig. 4*F*). These results suggest that depolarization of mitochondria by FCCP is not sufficient to produce ablation by itself but may slightly facilitate capsaicin-induced ablation through unknown mechanisms. Although capsaicin was suggested to directly depolarize mitochondria independent of TRPV1 in rat sensory neurons (34), it is unlikely that direct depolarization of mitochondria by capsaicin is a dominant factor. FCCP- or capsaicin-induced depolarization of mitochondria may diminish the Ca^{2+} sequestration capacity of mitochondria, which may result in prolonged accumulation of axonal Ca^{2+} and subsequent augmentation of the other Ca^{2+}-dependent mechanisms.

Because capsaicin-induced cell death is diminished by inhibition of mPTP (19), and the opening of mPTP is facilitated by ROS (38), we examined the contribution of mPTP and ROS to axonal ablation. However, cyclosporin A and TRO19622, inhibitors of mPTP (33), did not affect ablation. Furthermore, phenyl a-*tert*-butyl nitrone and the antioxidant supplement AOx (Sigma), ROS scavengers (39), did not affect ablation either (Fig. 4*G*). Overall, these results suggest that dissipation of the mitochondrial membrane potential and inhibition of mPTP or ROS are not critical contributors to capsaicin-induced ablation of TRPV1-expressing nerve terminals.

Inhibition of calpain substantially prevents capsaicin-induced ablation

Calpains are Ca^{2+}-dependent cysteine proteases that play critical roles in cell function (40). Abnormal activation of calpains has been associated with multiple disorders, such as traumatic brain injury, spinal cord injury, neurodegenerative diseases, and peripheral neuropathies (41). Because calpain is involved in Wallerian degeneration of axons (18, 42) and axonal beading (43), we tested the effects of calpain inhibitors on capsaicin-induced ablation. Pretreatment of axonal terminals with MDL28170 substantially attenuated, but did not eliminate, capsaicin-induced degeneration (Fig. 5, *A* and *C*). To confirm the effects of calpain inhibition, we tested calpain inhibitor I. However, calpain inhibitor I did not show significant reversal of

ablation (Fig. 5*C*). Because no calpain inhibitors are highly specific for calpains or individual calpain subtypes (40), we tested the effects of overexpression of calpastatin, an endogenously expressed specific inhibitor of calpain. Calpastatin is a suicide-inhibiting molecule of calpain that is known to affect Wallerian degeneration of sensory nerves by regulating calpain activity (44, 45). We overexpressed calpastatin in dissociated DRG neurons by electroporating cDNA encoding human calpastatin. When we overexpressed calpastatin in DRG neurons from TRPV1-GFP mice, capsaicin-induced ablation was decreased by half compared with the control (Fig. 5, *B* and *C*). The inhibitory effects of MDL28170 or calpastatin are unlikely to be derived from direct suppressive effects on the activation of TRPV1 because pretreatment with MDL or overexpression of calpastatin did not significantly affect capsaicin-induced Ca^{2+} responses in somata of sensory neurons (Fig. 5*D*).

Among 15 mammalian calpains, the best characterized calpains are calpain-1 (μ-calpain) and calpain-2 (m-calpain, a product of the CAPN2 gene) (40). We chose to test the effects of knocking down calpain-2 because our transcriptome analysis in sensory ganglia shows that calpain-2 is more abundantly expressed than calpain-1 (46). Calpain-2 is expressed both in large myelinated neurons and calcitonin gene-related peptide (CGRP)-positive neurons in DRG and up-regulated following neuropathic injury (47). After treatment of dissociated DRG neurons with RNAi against calpain-2, the expression of calpain-2 protein was significantly suppressed compared with a mismatch control (Fig. 5*E*). We treated the cultured neurons in the MFC with RNAi against calpain-2 or a mismatch control and performed time-lapse imaging to assess capsaicin-induced ablation after 2 days. Knockdown of calpain-2 slightly but significantly attenuated capsaicin-induced ablation ($p < 0.05$, log-rank test, Fig. 5*F*). The effect of siRNA was modest compared with that of MDL, which may be due to the incomplete knockdown of calpain-2 and contributions from other subtypes of calpain. Overall, these results suggest that activation of calpain induced by increased cytosolic Ca^{2+} following capsaicin-induced TRPV1 activation is a major Ca^{2+}-dependent mechanism of ablation.

A single injection of capsaicin induces ablation of TRPV1-lineage afferent terminals for weeks in vivo

To examine the mechanisms underlying capsaicin-induced ablation *in vivo*, we established an *in vivo* ablation assay in the hind paws of TRPV1-GFP mice. We injected capsaicin or vehicle subcutaneously into the right and left hind paws of TRPV1-GFP mice. Sections of plantar skin were immunostained using a GFP antibody (Fig. 6, *A* and *B*). The number of intraepidermal fibers in capsaicin-injected skin was reduced by ~20% after 6 h and by >40% after 1 day. Although maximal ablation was only ~40%, this likely reflects ablation of a majority of TRPV1-expressing fibers because only approximately half of the adult TRPV1-lineage neurons express TRPV1 because of developmental changes in TRPV1 expression (48). Capsaicin-induced ablation was substantial over a 4-week interval (Fig. 6*C*). The extent of ablation was substantially weaker at week 6, and the effect of capsaicin was found to be negligible by week 8 (Fig. 6*C*). When we quantified the proportion of TRPV1-lineage neurons among NeuN+ neurons within the L4 or L5 DRG, the capsaicin- or vehicle-injected side did not show a significant difference (Fig. 6, *D* and *E*; 53.7% ± 3.3% in Veh, 59.3% ± 2.8% in cap, $p > 0.4$, $n = 4$/group). These results suggest that capsaicin injected into the skin *in vivo* substantially ablates TRPV1-lineage afferent terminals for a prolonged period and that capsaicin-induced ablation is reversible and confined to the nociceptive terminals in the injected site without degeneration of the somata, consistent with previous findings reported for rat hind paws following injection of RTX (11, 13).

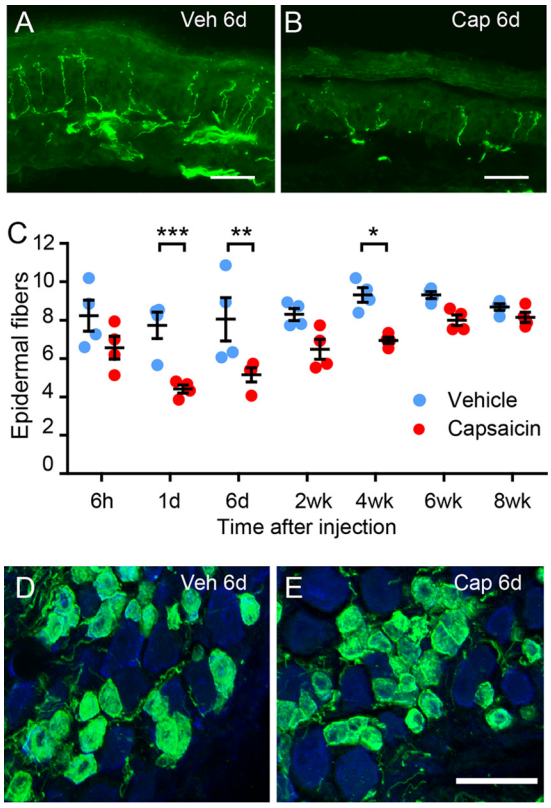

Figure 6. Capsaicin induces a month-long ablation of epidermal TRPV1-lineage fibers *in vivo*. *A* and *B*, examples of hind paw skin 6 days following the intraplantar injection of vehicle (*A*, 20 μl/25% PEG300 and 75% H_2O, left hind paw) or capsaicin (*B*, 10 μg in 20 μl of vehicle, right hind paw) in adult TRPV1-GFP mice. *Green signals* represent GFP labeled by specific antibody. *Scale bars* = 50 μm. *C*, time course of capsaicin-induced ablation *in vivo*. Vehicle or capsaicin was injected into left and right hind paws, respectively. The mice were euthanized after the indicated times. The numbers of GFP-positive epidermal fibers passing through the epidermis-dermis junction were counted in each image, and values from 15 images taken from the same hind paw were averaged. $n = 4$ mice/group. Data are presented as mean ± S.E. Two-way ANOVA followed by Bonferroni post-hoc test; *, $p < 0.05$; **, $p < 0.01$; ***, $p < 0.001$. *D* and *E*, examples of double labeling of GFP (*green*) or NeuN (*blue*) in lumbar DRG from TRPV1-GFP mice 6 days following intraplantar injection of vehicle (*D*) or capsaicin (*E*). *Scale bar* = 50 μm.

Capsaicin mediates ablation of TRPV1-lineage axonal terminals in vivo in a Ca^{2+}/calpain-dependent manner

To examine the mechanisms underlying capsaicin-induced ablation *in vivo*, we performed an *in vivo* ablation assay in the hind paws of TRPV1-GFP mice along with pharmacological manipulations (Fig. 7). Co-injection of EGTA with capsaicin (10 μg) attenuated capsaicin-induced ablation in the hind paws, consistent with other evidence indicating that capsaicin-induced ablation of TRPV1-lineage nociceptor terminals

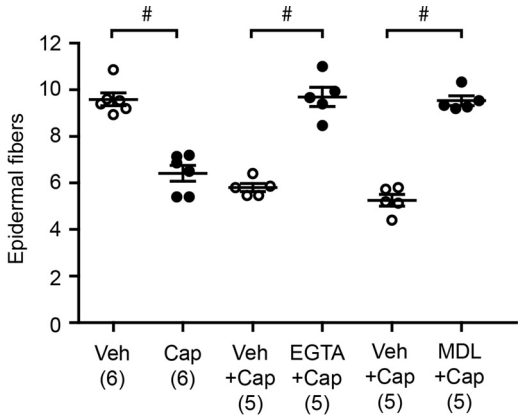

Figure 7. Capsaicin induces ablation of epidermal TRPV1-lineage fibers in a Ca^{2+}- and calpain-dependent manner *in vivo*. In adult TRPV1-GFP mice, 20 μl of Veh (25% PEG300 and 75% H_2O) or capsaicin (0.05% in Veh) was subcutaneously injected into the left (Veh) and right (Cap) hind paws, respectively. In other sets of mice, 20 μl of drug or vehicle was injected into the left and right hind paws along with capsaicin to test the effects of drugs on ablation as indicated. The animals were euthanized after a week, and intraepidermal GFP-expressing nerve terminals were quantified. *EGTA*, 10 mM EGTA in PBS (pH 7.4); *MDL*, 10 mM MDL28170 in DMSO. *Numbers in parentheses* represent the number of animals in each group. One-way ANOVA followed by Bonferroni post hoc analysis; #, $p < 0.0001$.

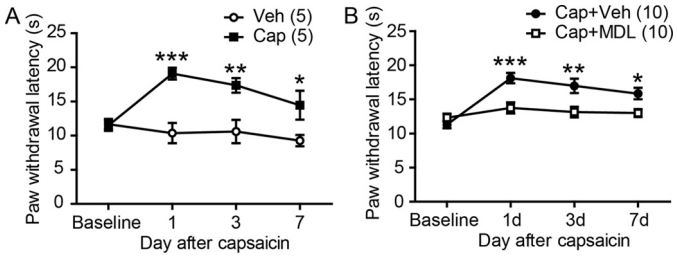

Figure 8. Inhibition of calpain attenuates capsaicin-induced thermal hypoalgesia. *A* and *B*, thermal sensitivity of hind paws in C57bl/6 mice before and after injection of vehicle or capsaicin (*A*) or capsaicin + Veh or capsaicin + MDL (*B*) into the left and right hind paws, respectively. ***, $p < 0.001$; **, $p < 0.01$; *, $p < 0.05$ in two-way repeated-measures ANOVA followed by Bonferroni post hoc analysis. *Numbers in parentheses* represent the numbers of mice in each group.

depends on Ca^{2+}. Co-injection of MDL28170 (200 nmol) also decreased the capsaicin-induced ablation of TRPV1-lineage axonal terminals in the skin.

Calpain mediates capsaicin-induced thermal hypoalgesia

Injection of vanilloids into the hind paw induces thermal hypoalgesia lasting for weeks (12), consistent with a capsaicin-induced ablation of TRPV1-expressing afferent terminals. For validation of calpain-dependent mechanisms, we examined the effects of MDL on capsaicin-induced thermal hypoalgesia in hind paws. When capsaicin (10 μg) was injected into the hind paw, the withdrawal latency to heat increased significantly beginning as early as day 1 and through the first week after injection (two-way repeated-measures ANOVA, Fig. 8*A*). In contrast, there was no significant change in the vehicle-injected paw. When capsaicin was injected along with MDL28170, the effects on latency were significantly less (two-way repeated-measure ANOVA, Fig. 8*B*). The anatomical (Fig. 7) and behavioral effects with MDL28170 together suggest that calpain contributes to capsaicin-induced nerve terminal ablation.

Discussion

To investigate the mechanisms of axonal ablation following capsaicin application, we established novel models for quantifying changes in TRPV1-lineage nerve terminals *in vitro*. This approach was optimal for our mechanistic study. First, the MFC allowed us to restrict the application of capsaicin to axons without exposure to somata, which excluded the possibility that axonal ablation could be a consequence of cell death. Second, changes in nerve terminals were quantified in real time so that axons before and after the application of capsaicin could be easily compared. Third, the assay did not involve a immunocytochemical staining procedure, which excluded any potential untoward effects of using antibodies against TRPV1 or neuropeptides, *e.g.* degradation or degranulation of proteins or altered specificity of antibody following exposure to capsaicin. Fourth, the assay was relatively high-throughput and allowed us to screen multiple pharmacological manipulations. For monitoring changes of TRPV1-lineage nerve terminals *in vivo*, we also used the TRPV1-lineage reporter mouse line and performed immunohistochemical labeling of intraepidermal fluorophore-positive fibers. The use of high-specificity antibodies against fluorophores unequivocally demonstrated ablation of nerve terminals and allowed for reliable quantification of intraepidermal TRPV1-lineage nerve terminals.

Investigators have speculated about Ca^{2+}-dependent mechanisms underlying vanilloid-induced axonal ablation, but little direct data have been introduced. Although Ca^{2+} influx was necessary and sufficient for capsaicin-induced ablation of nerve terminals of TRPV1-lineage afferents, we acknowledge the possibility that different mechanisms might contribute to capsaicin-induced ablation in nerve terminals observed in *in vitro* and *in vivo* models. One of the main differences relates to time course. Nerve terminals in the *in vitro* ablation assay in the MFC displayed almost full ablation within 10 min, whereas full ablation occurred more slowly (~1 day) *in vivo*. Multiple factors, including a different local environment around afferent terminals under these conditions, may underpin the difference. It is possible, therefore, that the mechanisms of ablation identified *in vitro* do not fully explain ablation *in vivo*. However, our data suggest that the major early events following activation of TRPV1 by capsaicin were the same *in vitro* and *in vivo*. Prevention of Ca^{2+} influx and calpain activation attenuated capsaicin-induced ablation *in vitro* and *in vivo*; thus, Ca^{2+} influx followed by activation of calpain likely constitutes one of the critical early events.

Our results indicated that Ca^{2+} influx through TRPV1, but not through VDCC or the ER, was a major contributor leading to capsaicin-induced ablation *in vitro* and *in vivo*. The reason for preferential coupling between TRPV1 and capsaicin-induced ablation was not determined, but there are several possibilities. First, capsaicin-induced TRPV1 might produce a greater and more prolonged cytosolic Ca^{2+} increase than KCl or thapsigargin. Second, perhaps capsaicin indirectly affects intra-axonal Ca^{2+} homeostasis. It is known that capsaicin affects mitochondrial function (34). Interference with mitochondrial function might enhance ablation. Third, it is possible that TRPV1 preferentially engages substrates involved in axonal integrity. For example, TRPV1 is known to directly

interact with microtubules (49). These mechanisms, singly or in aggregate, may contribute to prolonged maintenance of high levels of intracellular Ca^{2+} and preferential degradation of cytoskeletal components following influx of Ca^{2+} through TRPV1 upon activation by capsaicin.

Our results from FCCP/oligomycin suggested that Ca^{2+} release from mitochondria alone or depolarization of mitochondrial membrane potential was not sufficient to induce ablation of TRPV1-lineage terminals. These results do not exclude a contribution of mitochondria, however, and our data do not necessarily contradict a recent report suggesting a role for mitochondria in capsaicin-induced degeneration of axons (21). Capsaicin increases mitochondrial fission, which, in turn, decreases mitochondrial stationary site sizes in a Ca^{2+}-dependent manner. Prevention of mitochondrial fission decreases capsaicin-induced degeneration *in vitro* (21). Although it is unclear how mitochondrial fission is mechanistically associated with axonal ablation, our data at least suggest that depolarization of the mitochondrial membrane potential, opening of mPTP, or generation of ROS may not be dominant causative factors. Alternatively, fission or other mitochondrial damage may reduce the capacity of mitochondria to segregate cytosolic Ca^{2+} within axons, which, in turn, might augment other, Ca^{2+}-dependent pathways, *e.g.* calpain. Our data also suggest differential roles of mPTP in capsaicin-induced peripheral ablation *versus* neuronal death at the soma level (19). In somata, opening of mPTP might lead to apoptosis by releasing proapoptotic proteins or activating the caspase cascade. These same mechanisms may not apply at the axonal level. Opening of mPTP contributes to axonal degeneration of explanted sciatic nerve independent of effects on the soma (33). Also, similar Ca^{2+}-dependent mechanisms, underlying capsaicin-induced axonal ablation, may be distinct from those of Wallerian degeneration. Notably, capsaicin-induced axonal ablation apparently occurs much faster (10 min *in vitro*, 1 day *in vivo*) than axotomy-induced Wallerian degeneration (~6 days *ex vivo*). Following exposure to vanilloids, the intra-axonal Ca^{2+} increase is an initial event leading to ablation processes, whereas axotomy-induced degeneration follows a slower time scale. Fast elevation of Ca^{2+} following capsaicin application likely induces rapid "chemical axotomy" at localized spots of axonal terminals, which might be followed by Wallerian degeneration-like processes within ablated axonal fragments. Mechanical axotomy upstream likely does not engage the same degree of immediate Ca^{2+} influx distally. Therefore, we presume that the mechanisms underlying capsaicin-induced ablation are distinct from axonal degeneration from other injury.

Pharmacological inhibition of calpain is known to attenuate capsaicin-induced cell death of dissociated sensory neurons (18). Our results extend these findings and demonstrate that calpain is a major contributor mediating capsaicin-induced ablation of nociceptor terminals *in vitro* and *in vivo*. Capsaicin-induced activation of TRPV1 induces Ca^{2+} influx at nerve terminals, which, in turn, activates calpain, likely calpain-2, leading to axonal ablation of TRPV1-expressing afferents and concomitant thermal hypoalgesia. Because cytoskeletal components such as neurofilaments and microtubules are well known proteolytic targets of calpains (40, 50), Ca^{2+}-dependent activation of calpains contributes to execution of axonal degeneration following axonal injury (41) and. likely, capsaicin-induced ablation. Considering the complicated molecular mechanisms involved in axonal degeneration under various pathologies or injuries (20, 23), we expect that capsaicin-induced ablation also involves multiple overlapping yet unique molecular mechanisms. Using the *in vitro* and *in vivo* methods established in this project, we will continue to examine signaling associated with capsaicin-induced ablation of TRPV1-expressing nerve terminals. An important question is whether the identified mechanisms underlying capsaicin-induced ablation of axonal terminals are actually associated with therapeutic effects of capsaicin. It is clear that further work in this area needs to be done. We expect that this study and future studies will help not only to better understand the mechanisms of capsaicin-induced analgesia but also to improve capsaicin therapy by enhancing therapeutic efficacy or through development of novel methods to enhance the positive effects of capsaicin while minimizing side effects.

Materials and methods

Animals

All procedures were conducted in accordance with the National Institutes of Health Guide for the Care and Use of Laboratory Animals and were performed under a University of Maryland-approved Institutional Animal Care and Use Committee protocol. To visualize TRPV1-lineage axons, we used a genetically engineered mouse model that expresses a membrane-bound fluorophore selectively in TRPV1-expressing neurons. We crossed two lines of genetically engineered mice: first, $TRPV1^{Cre}$ ($TRPV1^{tm1(cre)Bbm}$/J, The Jackson Laboratory, stock no. 017769), in which Cre recombinase is expressed under the control of the TRPV1 promoter (48); second, $ROSA^{mT/mG}$ ($Gt(ROSA)26^{Sortm4(ACTB-tdTomato,-EGFP)}$Luo/J, The Jackson Laboratory, stock no. 007676), which constitutively express tdTomato in every cell without Cre recombination (51). The offspring express membrane-tethered enhanced GFP in neurons expressing Cre recombinase, which permits identification of TRPV1-lineage neurons by GFP signals (TRPV1-GFP mice). In some experiments, we crossed the $TRPV1^{Cre}$ with $ROSA^{tomato}$ ($Gt(ROSA)26^{Sortm14(CAG-tdTomato)Hze}$/J, The Jackson Laboratory, stock no. 007914) mice. The offspring (TRPV1-Tomato mice) express tdTomato in neurons expressing Cre recombinase, which allows identification of TRPV1-lineage neurons by tdTomato signals. We also used TRPV1 KO mice ($TRPV1^{tm1jul}$/J, The Jackson Laboratory, stock no. 003770) and C57BL/6 mice (The Jackson Laboratory, stock no. 000664). All experiments were carried out on adult mice (22–30 g).

Culture of DRG neurons in MFC

We cultured DRG neurons in microfluidic devices (Xona Microfluidics) following the instructions of the manufacturer (Fig. 1*A*). It was reported that somata and axons of DRG neurons were successfully segregated and independently manipulated using this system (22). Autoclaved rectangular glass coverslips were coated with poly-D-ornithine and laminin. Microfluidic devices (SND150 with 150-μm microgrooves or TCND500 with 500-μm microgrooves) were autoclaved,

attached to the glass coverslip, and kept in 100-mm culture plates. Primary sensory neurons were dissociated from adult mice as described previously (52). Mice (4–9 weeks old) were anesthetized using a mixture of ketamine (80 mg/kg) and xylazine (10 mg/kg). Dorsal root ganglia were dissected out and collected in cold Puck's saline (171 mM NaCl, 6.7 mM KCl, 1.4 mM Na_2HPO_4, 0.5 mM KH_2PO_4, and 6.0 mM glucose (pH 7.3)). The ganglia were incubated in 5 ml of DMEM/F12 medium containing collagenase type IV (1 mg/ml) at 37 °C for 30 min. The ganglia were incubated for an additional 15 min following addition of trypsin (0.25%) and EDTA (0.025%). The tissues were triturated with flame-polished Pasteur pipettes. After spinning down, the neurons were resuspended in DMEM/F12 medium containing 10% FBS, 1% penicillin/streptomycin/Fungizone and plated into the chamber. DRG neurons dissociated from one mouse were plated into five chambers. The neurons were maintained in DMEM/F12 containing 10% FBS, 1% penicillin/streptomycin/Fungizone at 37 °C in a 5% CO_2 incubator. The culture medium was replaced every 3 days.

Electroporation of dissociated DRG neurons

Plasmids containing cDNA encoding GFP in pMax (Lonza) in pCMV6-entry (Origene), mito-LAR-GECO1.2 in pBAD/His B (a generous gift from Dr. Robert Campbell, University of Alberta) (53), or empty vector (pcDNA3) were transfected using an electroporator (Nucleofector 4D, *x* axis, Lonza) as described previously (52). Following electroporation, dissociated neurons were plated onto glass coverslips (8-mm diameter) coated with poly-ornithine and laminin for Ca^{2+} imaging or into MFC for axonal imaging. Ca^{2+} imaging was performed after 2–3 days, and axonal imaging in MFC was performed after about 2 weeks.

Time-lapse imaging of axonal terminals

Time-lapse imaging of axonal terminals expressing GFP or tdTomato was performed 13–15 days following plating on MFC. The medium was replaced with imaging buffer (130 mM NaCl, 3 mM KCl, 0.5 mM $MgCl_2$, 0.9 mM $CaCl_2$, 10 mM HEPES, 10 mM sucrose, and 1.2 mM $NaHCO_3$ (pH 7.45, 320 mosmol, adjusted with mannitol)) and kept for 30 min at 37 °C in a 5% CO_2 incubator. For imaging, the chamber was placed on the stage of an inverted epifluorescence microscope (Axiovert 200 M microscope, Zeiss), and the imaging buffer was replaced with fresh imaging buffer containing vehicle or testing drug. Acquisition of fluorescence images was initiated immediately prior to addition of capsaicin to a well in the axonal compartment. Capsaicin was added alone or together with vehicle or testing drug. Images were taken 1, 3, 10, 19, and 28 min after addition of capsaicin. To quantify fibers undergoing changes following capsaicin application, the observer was blinded to the experimental groups. Because the axonal terminals were heavily branched in the axonal compartment, it was difficult to clearly tease out changes of individual fibers. To minimize complexity, we followed the methods below. Instead of analyzing the entire image, we limited our analysis to the region of interest (50- to 100-μm high) over the area containing the highest density of nerve terminals before addition of capsaicin. Within the region of interest, we visually identified apparent individual fibers showing continuity so that different segments within the apparent identical fiber were not counted twice. Each fiber was monitored when beading or blebbing, disruption of continuity, or fragmentation occurred. When any one of these signs was shown, the fiber was considered to be affected. If no such signs occurred, the fiber was counted as unaffected. For each fiber, the time point of the abnormal appearance was noted. To minimize overestimation of affected fibers, aggregated affected fibers were counted as one. To compare the proportion of unaffected GFP+ fibers in different groups, Kaplan-Meier survival curves were generated in each group using Prism software (GraphPad). Survival proportion was plotted as mean ± S.E. Survival curves from different groups were compared by log-rank test. Data in each experimental group were obtained from at least three independent experimental repeats.

Ca^{2+} imaging assay

To monitor changes in cytosolic Ca^{2+}, we performed ratiometric Ca^{2+} imaging using Fura-2/AM as described previously (52). After 1 day following dissociation, DRG neurons were loaded with Fura-2/AM for 40 min at 37 °C in calcium imaging buffer (130 mM NaCl, 3 mM KCl, 0.5 mM $MgCl_2$, 0.9 mM $CaCl_2$, 10 mM HEPES, 10 mM sucrose, and 1.2 mM $NaHCO_3$ (pH 7.45, 320 mosmol adjusted with mannitol)). Ratiometric Ca^{2+} imaging was performed using an inverted fluorescence microscope (Eclipse Ti, Nikon, Melville, NY), optical filter changer (Lambda 10-B, Sutter Instruments), and charge-coupled device camera (Nikon). After a 15-min wash period for de-esterification, dual images (excitation at 340 and 380 nm, emission at 510 nm) were collected every 2 s using NIS Elements (Nikon). The Fura response was defined as the ratio of background-subtracted emissions measured during excitation at 340 and 380 nm. To monitor changes in mitochondria Ca^{2+} level, we used the genetically encoded Ca^{2+} sensor mito-LAR-GECO1.2 containing a mitochondrial targeting sequence (53). Two days after transfection of mito-LAR-GECO1.2, the neurons were loaded with Fura-2/AM for simultaneous recording of cytosolic and mitochondrial Ca^{2+} changes. Fluorescence was excited at 340, 380, and 550 nm every 5 s. Fluorescence emission was collected with a dual-band emission filter (FF01-512/630, Semrock). The mitochondrial Ca^{2+} response was calculated as the relative ratio to the baseline prior to drug application. Data in each experimental group were obtained from at least four independent experimental repeats.

Electrophysiology

HEK293 cells were cultured and transfected using Lipofectamine 2000 (Invitrogen) as described previously (52). Plasmids containing cDNA encoding rat TRPV1 were cotransfected with cDNA-encoding mCherry. Transiently transfected HEK293 cells were replated onto poly-L-ornithine-coated coverslips and used for electrophysiological experiments after 16–26 h. Whole-cell voltage clamp techniques were performed as described previously (52, 54). The pipettes were filled with internal solution (150 mM NaOH, 1 mM $MgCl_2$, 10 mM HEPES, and 5 mM EGTA (pH 7.4) adjusted with HCl). The recording bath contained external solution (140 mM NaCl, 5 mM KCl, 2

mM $CaCl_2$, 1 mM $MgCl_2$, 10 mM HEPES, and 10 mM glucose (pH 7.4) adjusted with NaOH).

Immunohistochemical analysis of TRPV1-lineage afferent terminals

To assess capsaicin-induced ablation of TRPV1-lineage nerve terminals *in vivo*, we performed immunohistochemical analysis in skin following injection of capsaicin. In adult TRPV1-GFP mice, hind paws were injected with either vehicle (20 μl, 25% PEG300 and 75% H_2O) or capsaicin (10 μg in 20 μl of vehicle). For consistency, injections were performed under anesthesia (80 mg/kg ketamine, 10 mg/kg xylazine). At the times indicated under "Results," animals were euthanized and perfused transcardially using 3.7% formaldehyde in phosphate-buffered saline. Skin was cryoprotected in sucrose and cryosectioned (30 μm). Immunohistochemistry was performed using a specific antibody against GFP (1:1000, rabbit polyclonal; A11122, Invitrogen) (55) or red fluorescent protein (RFP) (for detecting tdTomato, 1:1000, rabbit polyclonal, 600-401-379, Rockland) (56). For quantifying epidermal fibers, 3 images/tissue section and 5 sections/hind paw (total, 15 images from one hind paw) were examined. The numbers of epidermal fibers passing through the epidermis-dermis junction were counted in each image, and values from 15 images were averaged.

siRNA and Western blot analysis

Mouse DRG were dissociated and plated in a 12-well plate. The cultures were treated with negative control siRNA (AATTCTCCGAACGTCTCACGT) or siRNA against calpain-2 (GCGGTCAGATACCTTCATCAA) manufactured by Qiagen. The effect of the siRNA against calpain-2 was validated in primary neurons (57). The oligos (100 nM) were transfected using Lipofectamine 2000 (Invitrogen). The cultures were incubated for 2 days before testing. For determining the extent of knockdown, we performed Western blot analysis. The cultures were lysed via lysis buffer that included a protease inhibitor mixture. Lysate concentration was determined using a Bio-Rad protein assay kit. The protein sample/loading buffer was denatured at 100 °C for 5 min and separated by 4–12% NuPAGE gel. Protein was blotted onto a PVDF membrane. The membrane was blocked with 5% skim milk for 1 h at room temperature. The membrane was incubated with antibody against calpain-2 (1:1000, rabbit polyclonal, PA5-17494, Thermo Fisher) or GAPDH (1:20,000, mouse monoclonal, CB1001, Calbiochem). The specificity of the calpain-2 antibody was verified previously (57). Primary antibodies were detected using horseradish peroxidase-conjugated anti-rabbit or anti-goat IgG antibodies. Bands were visualized with ECL Western blotting detection reagents (Amersham Biosciences) and recorded on X-ray film. The band signals on the film were scanned and quantified with ImageJ software. By exposing the film for different durations, we confirmed that the intensity of the band was not saturated under our conditions. For the relative quantification of calpain-2, the GAPDH level of the corresponding sample was used as the normalization control. The expression level of GAPDH was not different among the naïve control, control RNAi, and CAPN2 RNAi groups.

Hargreaves assay for measuring thermal sensitivity in hind paw

The mice were acclimated to the testing environment for 2 days. The mice were placed on the glass platform of a Hargreaves device (PAW Thermal Stimulator, University of California, San Diego, CA) under an acrylic box for at least 30 min for habituation. For testing, the mice were placed on the glass platform under an acrylic box for 10 min until they were settled down. The baseline latency of the radiant heat source was adjusted to a range of 10–12 s with a cutoff time of 20.5 s to prevent tissue damage. To record paw withdrawal latency in response to the heat stimulus, both hind paws were measured three times with a 10-min interval, and the average latency of three withdrawals was used for analysis. The experimenter performing the procedure was blinded to the experimental group status of the mouse.

Drugs

Ru360 was purchased from Millipore, and A01, TC AQP, and TGN020 were from Tocris. All other chemicals and drugs were purchased from Sigma-Aldrich. The drugs were dissolved directly in imaging buffer at the final concentration or in DMSO at a >1000-fold excess of the final concentration. For testing the effects of drugs in the *in vitro* ablation assay, groups of several drugs were compared with their respective vehicle controls. For testing the effects of pharmacological manipulations on capsaicin-induced ablation of afferent terminals *in vivo*, we injected inhibitors into one hind paw and vehicle into the other hind paw prior to capsaicin injection. The animals were euthanized after 6–7 days for immunohistochemical assessment of intraepidermal fiber density in hind paw glabrous skin. To determine the role of calpain, we injected 20 μl of 10 mM MDL28170 (200 nmol), which is an intermediate dose between the systemic and intraspinal doses preventing inflammation-induced neurofilament breakdown in rats (50).

Data analysis

Statistical analyses were performed using Prism 5 (GraphPad). Mean values between two groups were compared using Student's *t* test. Proportions of unaffected fibers (survival curves) in different groups were compared using log-rank test. Concentration-dependent relationships were fitted using a sigmoidal equation: $Y = \text{bottom} + (\text{top-bottom})/(1 + 10^{((\log(IC50)-X)*H)})$, where top and bottom are maximal and minimal plateaus of responses, IC_{50} is the concentration of agonist that gives a response halfway between bottom and top, and H is the Hill slope. The numbers in experimental groups were included in the graphs either inside columns or in parentheses next to group names.

Author contributions—M. K. C. and J. N. C. conceived the study and wrote the manuscript. M. K. C., F. W., and J. Y. R. designed the experiments. Sheng Wang, Sen Wang, J. A., J. J., and M. K. C. performed the experiments and analyzed the data. All authors reviewed the results and approved the final version of the manuscript.

Acknowledgments—We thank Drs. Michael Caterina and Ohannes Melemedjian for helpful suggestions and Youping Zhang, Alisha Karley, and Bri'Anna Horne for technical assistance.

References

1. Caterina, M. J., Schumacher, M. A., Tominaga, M., Rosen, T. A., Levine, J. D., and Julius, D. (1997) The capsaicin receptor: a heat-activated ion channel in the pain pathway. *Nature* **389,** 816–824
2. Szallasi, A., and Blumberg, P. M. (1999) Vanilloid (capsaicin) receptors and mechanisms. *Pharmacol Rev.* **51,** 159–212
3. Iadarola, M. J., and Gonnella, G. L. (2013) Resiniferatoxin for pain treatment: an interventional approach to personalized pain medicine. *Open Pain J.* **6,** 95–107
4. Mou, J., Paillard, F., Turnbull, B., Trudeau, J., Stoker, M., and Katz, N. P. (2013) Efficacy of Qutenza® (capsaicin) 8% patch for neuropathic pain: a meta-analysis of the Qutenza Clinical Trials Database. *Pain* **154,** 1632–1639
5. Campbell, C. M., Diamond, E., Schmidt, W. K., Kelly, M., Allen, R., Houghton, W., Brady, K. L., and Campbell, J. N. (2016) A randomized, double blind, placebo controlled trial of injected capsaicin for pain in Morton's neuroma. *Pain* **157,** 1297–1304
6. Chung, M. K., and Campbell, J. N. (2016) Use of capsaicin to treat pain: mechanistic and therapeutic considerations. *Pharmaceuticals* **9,** E66
7. Anand, P., and Bley, K. (2011) Topical capsaicin for pain management: therapeutic potential and mechanisms of action of the new high-concentration capsaicin 8% patch. *Br. J. Anaesth.* **107,** 490–502
8. Borbiro, I., Badheka, D., and Rohacs, T. (2015) Activation of TRPV1 channels inhibits mechanosensitive Piezo channel activity by depleting membrane phosphoinositides. *Sci. Signal.* **8,** ra15
9. Liu, L., Oortgiesen, M., Li, L., and Simon, S. A. (2001) Capsaicin inhibits activation of voltage-gated sodium currents in capsaicin-sensitive trigeminal ganglion neurons. *J. Neurophysiol.* **85,** 745–758
10. Ma, X. L., Zhang, F. X., Dong, F., Bao, L., and Zhang, X. (2015) Experimental evidence for alleviating nociceptive hypersensitivity by single application of capsaicin. *Mol. Pain* **11,** 22
11. Karai, L., Brown, D. C., Mannes, A. J., Connelly, S. T., Brown, J., Gandal, M., Wellisch, O. M., Neubert, J. K., Olah, Z., and Iadarola, M. J. (2004) Deletion of vanilloid receptor 1-expressing primary afferent neurons for pain control. *J. Clin. Invest.* **113,** 1344–1352
12. Neubert, J. K., Karai, L., Jun, J. H., Kim, H. S., Olah, Z., and Iadarola, M. J. (2003) Peripherally induced resiniferatoxin analgesia. *Pain* **104,** 219–228
13. Yu, S., and Premkumar, L. S. (2015) Ablation and regeneration of peripheral and central TRPV1 expressing nerve terminals and the consequence of nociception. *Open Pain J.* **8,** 1–9
14. Simone, D. A., Nolano, M., Johnson, T., Wendelschafer-Crabb, G., and Kennedy, W. R. (1998) Intradermal injection of capsaicin in humans produces degeneration and subsequent reinnervation of epidermal nerve fibers: correlation with sensory function. *J. Neurosci.* **18,** 8947–8959
15. Malmberg, A. B., Mizisin, A. P., Calcutt, N. A., von Stein, T., Robbins, W. R., and Bley, K. R. (2004) Reduced heat sensitivity and epidermal nerve fiber immunostaining following single applications of a high-concentration capsaicin patch. *Pain* **111,** 360–367
16. Polydefkis, M., Hauer, P., Sheth, S., Sirdofsky, M., Griffin, J. W., and McArthur, J. C. (2004) The time course of epidermal nerve fibre regeneration: studies in normal controls and in people with diabetes, with and without neuropathy. *Brain* **127,** 1606–1615
17. Caudle, R. M., Karai, L., Mena, N., Cooper, B. Y., Mannes, A. J., Perez, F. M., Iadarola, M. J., and Olah, Z. (2003) Resiniferatoxin-induced loss of plasma membrane in vanilloid receptor expressing cells. *Neurotoxicology* **24,** 895–908
18. Chard, P. S., Bleakman, D., Savidge, J. R., and Miller, R. J. (1995) Capsaicin-induced neurotoxicity in cultured dorsal root ganglion neurons: involvement of calcium-activated proteases. *Neuroscience* **65,** 1099–1108
19. Shin, C. Y., Shin, J., Kim, B. M., Wang, M. H., Jang, J. H., Surh, Y. J., and Oh, U. (2003) Essential role of mitochondrial permeability transition in vanilloid receptor 1-dependent cell death of sensory neurons. *Mol. Cell Neurosci.* **24,** 57–68
20. Neukomm, L. J., and Freeman, M. R. (2014) Diverse cellular and molecular modes of axon degeneration. *Trends Cell Biol.* **24,** 515–523
21. Chiang, H., Ohno, N., Hsieh, Y. L., Mahad, D. J., Kikuchi, S., Komuro, H., Hsieh, S. T., and Trapp, B. D. (2015) Mitochondrial fission augments capsaicin-induced axonal degeneration. *Acta Neuropathol.* **129,** 81–96
22. Tsantoulas, C., Farmer, C., Machado, P., Baba, K., McMahon, S. B., and Raouf, R. (2013) Probing functional properties of nociceptive axons using a microfluidic culture system. *PLoS ONE* **8,** e80722
23. Saxena, S., and Caroni, P. (2007) Mechanisms of axon degeneration: from development to disease. *Prog. Neurobiol.* **83,** 174–191
24. Zhai, Q., Wang, J., Kim, A., Liu, Q., Watts, R., Hoopfer, E., Mitchison, T., Luo, L., and He, Z. (2003) Involvement of the ubiquitin-proteasome system in the early stages of Wallerian degeneration. *Neuron* **39,** 217–225
25. Cavanaugh, D. J., Chesler, A. T., Jackson, A. C., Sigal, Y. M., Yamanaka, H., Grant, R., O'Donnell, D., Nicoll, R. A., Shah, N. M., Julius, D., and Basbaum, A. I. (2011) Trpv1 reporter mice reveal highly restricted brain distribution and functional expression in arteriolar smooth muscle cells. *J. Neurosci.* **31,** 5067–5077
26. George, E. B., Glass, J. D., and Griffin, J. W. (1995) Axotomy-induced axonal degeneration is mediated by calcium influx through ion-specific channels. *J. Neurosci.* **15,** 6445–6452
27. Kárai, L. J., Russell, J. T., Iadarola, M. J., and Oláh, Z. (2004) Vanilloid receptor 1 regulates multiple calcium compartments and contributes to Ca^{2+}-induced Ca^{2+} release in sensory neurons. *J. Biol. Chem.* **279,** 16377–16387
28. Villegas, R., Martinez, N. W., Lillo, J., Pihan, P., Hernandez, D., Twiss, J. L., and Court, F. A. (2014) Calcium release from intra-axonal endoplasmic reticulum leads to axon degeneration through mitochondrial dysfunction. *J. Neurosci.* **34,** 7179–7189
29. Takayama, Y., Uta, D., Furue, H., and Tominaga, M. (2015) Pain-enhancing mechanism through interaction between TRPV1 and anoctamin 1 in sensory neurons. *Proc. Natl. Acad. Sci. U.S.A.* **112,** 5213–5218
30. Schattling, B., Steinbach, K., Thies, E., Kruse, M., Menigoz, A., Ufer, F., Flockerzi, V., Brück, W., Pongs, O., Vennekens, R., Kneussel, M., Freichel, M., Merkler, D., and Friese, M. A. (2012) TRPM4 cation channel mediates axonal and neuronal degeneration in experimental autoimmune encephalomyelitis and multiple sclerosis. *Nat. Med.* **18,** 1805–1811
31. Shutov, L. P., Kim, M. S., Houlihan, P. R., Medvedeva, Y. V., and Usachev, Y. M. (2013) Mitochondria and plasma membrane Ca^{2+}-ATPase control presynaptic Ca^{2+} clearance in capsaicin-sensitive rat sensory neurons. *J. Physiol.* **591,** 2443–2462
32. Duchen, M. R. (2004) Roles of mitochondria in health and disease. *Diabetes* **53,** S96–102
33. Barrientos, S. A., Martinez, N. W., Yoo, S., Jara, J. S., Zamorano, S., Hetz, C., Twiss, J. L., Alvarez, J., and Court, F. A. (2011) Axonal degeneration is mediated by the mitochondrial permeability transition pore. *J. Neurosci.* **31,** 966–978
34. Dedov, V. N., Mandadi, S., Armati, P. J., and Verkhratsky, A. (2001) Capsaicin-induced depolarisation of mitochondria in dorsal root ganglion neurons is enhanced by vanilloid receptors. *Neuroscience* **103,** 219–226
35. Stout, A. K., Raphael, H. M., Kanterewicz, B. I., Klann, E., and Reynolds, I. J. (1998) Glutamate-induced neuron death requires mitochondrial calcium uptake. *Nat. Neurosci.* **1,** 366–373
36. Budd, S. L., and Nicholls, D. G. (1996) A reevaluation of the role of mitochondria in neuronal Ca^{2+} homeostasis. *J. Neurochem.* **66,** 403–411
37. Jackson, J. G., and Thayer, S. A. (2006) Mitochondrial modulation of Ca^{2+}-induced Ca^{2+} release in rat sensory neurons. *J. Neurophysiol.* **96,** 1093–1104
38. Halestrap, A. P. (2009) What is the mitochondrial permeability transition pore? *J. Mol. Cell. Cardiol.* **46,** 821–831
39. Kim, H. K., Zhang, Y. P., Gwak, Y. S., and Abdi, S. (2010) Phenyl *N*-*tert*-butylnitrone, a free radical scavenger, reduces mechanical allodynia in chemotherapy-induced neuropathic pain in rats. *Anesthesiology* **112,** 432–439
40. Goll, D. E., Thompson, V. F., Li, H., Wei, W., and Cong, J. (2003) The calpain system. *Physiol. Rev.* **83,** 731–801
41. Ma, M. (2013) Role of calpains in the injury-induced dysfunction and degeneration of the mammalian axon. *Neurobiol. Dis.* **60,** 61–79

42. Conforti, L., Gilley, J., and Coleman, M. P. (2014) Wallerian degeneration: an emerging axon death pathway linking injury and disease. *Nat. Rev. Neurosci.* **15,** 394–409
43. Kilinc, D., Gallo, G., and Barbee, K. A. (2009) Mechanical membrane injury induces axonal beading through localized activation of calpain. *Exp. Neurol.* **219,** 553–561
44. Yang, J., Weimer, R. M., Kallop, D., Olsen, O., Wu, Z., Renier, N., Uryu, K., and Tessier-Lavigne, M. (2013) Regulation of axon degeneration after injury and in development by the endogenous calpain inhibitor calpastatin. *Neuron* **80,** 1175–1189
45. Ma, M., Ferguson, T. A., Schoch, K. M., Li, J., Qian, Y., Shofer, F. S., Saatman, K. E., and Neumar, R. W. (2013) Calpains mediate axonal cytoskeleton disintegration during Wallerian degeneration. *Neurobiol. Dis.* **56,** 34–46
46. Chung, M. K., Park, J., Asgar, J., and Ro, J. Y. (2016) Transcriptome analysis of trigeminal ganglia following masseter muscle inflammation in rats. *Mol. Pain* **12,** 1744806916668526
47. Zang, Y., Chen, S. X., Liao, G. J., Zhu, H. Q., Wei, X. H., Cui, Y., Na, X. D., Pang, R. P., Xin, W. J., Zhou, L. J., and Liu, X. G. (2015) Calpain-2 contributes to neuropathic pain following motor nerve injury via up-regulating interleukin-6 in DRG neurons. *Brain Behav. Immun.* **44,** 37–47
48. Cavanaugh, D. J., Chesler, A. T., Bráz, J. M., Shah, N. M., Julius, D., and Basbaum, A. I. (2011) Restriction of transient receptor potential vanilloid-1 to the peptidergic subset of primary afferent neurons follows its developmental downregulation in nonpeptidergic neurons. *J. Neurosci.* **31,** 10119–10127
49. Goswami, C., Dreger, M., Jahnel, R., Bogen, O., Gillen, C., and Hucho, F. (2004) Identification and characterization of a Ca^{2+}-sensitive interaction of the vanilloid receptor TRPV1 with tubulin. *J. Neurochem.* **91,** 1092–1103
50. Kunz, S., Niederberger, E., Ehnert, C., Coste, O., Pfenninger, A., Kruip, J., Wendrich, T. M., Schmidtko, A., Tegeder, I., and Geisslinger, G. (2004) The calpain inhibitor MDL 28170 prevents inflammation-induced neurofilament light chain breakdown in the spinal cord and reduces thermal hyperalgesia. *Pain* **110,** 409–418
51. Muzumdar, M. D., Tasic, B., Miyamichi, K., Li, L., and Luo, L. (2007) A global double-fluorescent Cre reporter mouse. *Genesis* **45,** 593–605
52. Wang, S., Joseph, J., Ro, J. Y., and Chung, M. K. (2015) Modality-specific mechanisms of protein kinase C-induced hypersensitivity of TRPV1: S800 is a polymodal sensitization site. *Pain* **156,** 931–941
53. Wu, J., Prole, D. L., Shen, Y., Lin, Z., Gnanasekaran, A., Liu, Y., Chen, L., Zhou, H., Chen, S. R., Usachev, Y. M., Taylor, C. W., and Campbell, R. E. (2014) Red fluorescent genetically encoded Ca^{2+} indicators for use in mitochondria and endoplasmic reticulum. *Biochem. J.* **464,** 13–22
54. Wang, S., Lee, J., Ro, J. Y., and Chung, M. K. (2012) Warmth suppresses and desensitizes damage-sensing ion channel TRPA1. *Mol. Pain* **8,** 22
55. Chung, M. K., Jue, S. S., and Dong, X. (2012) Projection of non-peptidergic afferents to mouse tooth pulp. *J. Dent. Res.* **91,** 777–782
56. Stantcheva, K. K., Iovino, L., Dhandapani, R., Martinez, C., Castaldi, L., Nocchi, L., Perlas, E., Portulano, C., Pesaresi, M., Shirlekar, K. S., de Castro Reis, F., Paparountas, T., Bilbao, D., and Heppenstall, P. A. (2016) A subpopulation of itch-sensing neurons marked by Ret and somatostatin expression. *EMBO Rep.* **17,** 585–600
57. Wang, Y., Briz, V., Chishti, A., Bi, X., and Baudry, M. (2013) Distinct roles for mu-calpain and m-calpain in synaptic NMDAR-mediated neuroprotection and extrasynaptic NMDAR-mediated neurodegeneration. *J. Neurosci.* **33,** 18880–18892